Bimodal velocity distributions after ultraviolet-laser-induced desorption of NO from oxide surfaces. Experiments and results of model calculations

Th. Mull, B. Baumeister, M. Menges, and H.-J. Freund
Lehrstuhl für Physikalische Chemie I, Ruhr-Universität Bochum, Universitätsstrasse 150, 4630 Bochum, Germany

D. Weide, C. Fischer, and P. Andresen
Max-Planck-Institut für Strömungsforschung, Bunsenstrasse 10, 3400 Göttingen, Germany

(Received 13 November 1991; accepted 17 January 1992)

After UV-laser-induced desorption we observe bimodal velocity distributions independent of internal vibrational excitation [up to $v = 2$ (4%)] applying resonance-enhanced multiphoton ionization techniques. Both contributing desorption channels are of nonthermal origin. We introduce a model where the two desorption channels are correlated with the rupture of the molecule surface bond of the librating molecule either on the way toward or away from the surface. We have performed trajectory calculations to simulate the desorption processes. The calculated momentum distributions of the desorbing molecules show either one or two maxima, depending on lifetime, in agreement with experimental results. The vibrational distribution of the desorbing molecules can be reproduced by assuming transition into a state that is characterized by an altered N–O bond length as it is found, for example, in NO^-. The model calculations both for velocity distributions and vibrational excitations result in similar lifetimes of the excited state, even though the translational and the vibrational degree of freedom of the desorbing molecules are decoupled.

I. INTRODUCTION

Via the application of laser-induced fluorescence and resonance-enhanced multiphoton ionization (REMPI) in recent years rotational vibrational state resolved time-of-flight measurements of molecules desorbing from solid surfaces have been reported.[1-12]

The observation of nonthermal effects in this connection has stimulated theoretical efforts to understand the dynamics of photoinduced surface processes. Classical trajectory calculations as well as simulations applying the wave-packet approach have been performed to describe processes on metal surfaces.[13,14] We have studied UV-laser-induced desorption of NO from NiO(100) applying a REMPI method. The investigation of desorption phenomena from oxide surfaces is particularly appealing because the desorption cross section, at least for NO, is by orders of magnitude higher as compared to such process from metal surfaces [10^{-17} cm^2 vs 10^{-21} cm^2 (Refs. 15 and 16)]. In the next section we present experimental results which point toward the existence of two nonthermal desorption channels. So far we had assumed that only one of the observed desorption channels is of nonthermal origin. New data on well-characterized substrates described in the present and in following papers, however, have led us to extensions of our model[16] to account for the recent results indicating two nonthermal channels. To quantify our model assumptions we have performed trajectory calculations parallel to the experiments in order to simulate our results. We know that NO is weakly chemisorbed on NiO(100) with its axis inclined toward the surface normal,[17] and that the molecule executes a bending vibration. It is important whether the rupture of the surface–molecule bond happens while the molecule moves away from or toward the surface. These two possibilities lead to the appearence of bimodal velocity distributions. In Sec. III we describe the involved processes in more detail. Section IV collects some of the numerical results of the computer simulations and we discuss the experimental results on the basis of our theoretical calculations.

II. EXPERIMENTAL RESULTS

Figure 1 shows several velocity distributions (the transformation of the measured time-of-flight data into the shown velocity distributions is given in Appendix A) measured for different quantum numbers N of the angular momentum of the NO molecules desorbing from a thin NiO film with primary (100) orientation. These distributions were determined by a two-dimensional REMPI detection system (see Fig. 2) after desorption was stimulated by an ArF-excimer laser with 193 nm wavelength. The details of the experimental setup are described elsewhere.[18] Briefly, desorption is induced by the laser (ca. 2 mJ/cm^2; pulse duration 20–25 ns) at normal incidence to the surface. The desorbing particles are detected within a volume created by an excimer pumped dye laser (Lambda Physik, model LPD 3002) oriented parallel to the surface plane. The molecules within the volume are excited, and the ions are repelled into a drift tube and finally detected via a set of multichannel plates and a phosphor screen. The two-dimensional images can be stored via a computer-controlled video-camera. The experiments are carried out under 5×10^{-8} Torr NO background dosage so that the surface is automatically redosed. The repetition rate is 10 Hz. The signal is recorded applying a difference signal technique, described earlier.[5] The NO adsorbate on the thin NiO(100) film, which was grown on top of a Ni(100) single-crystal surface, was carefully characterized earlier, employing several techniques, such as x-ray photoe-

 0021-9606/92/097108-09$06.00

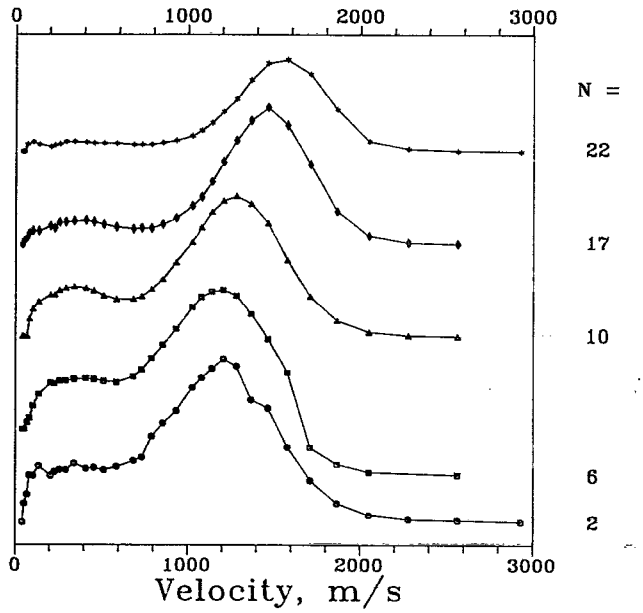

FIG. 1. Experimentally determined velocity flux distributions for different rotational quantum numbers (N) of NO in the first excited vibrational state ($v = 1$).

mission spectroscopy, ultraviolet photoemission spectroscopy, near-edge x-ray-absorption fine structure (NEXAFS), electron-energy-loss spectroscopy, and temperature-programmed desorption (TPD), etc.[17] In the following we shall use our knowledge of the adsorbate system to discuss and model the desorption dynamics.

The important message of Fig. 1 is that there are two maxima in the velocity distribution which show different dependences on the variation of angular momentum: The position of the maximum at lower velocity is independent of the rotational quantum number N, while the position of the maximum at higher velocities moves to higher velocities for larger rotational quanta. Very similar bimodal velocity distributions were obtained for all three lowest vibrational quanta ($v = 0,1,2$).

Figure 3 shows for one rotational state, i.e., $N = 10$, the velocity distributions for the three lowest vibrational states. From the population of the vibrational quanta a vibrational temperature may be estimated as $T_v = 1890 \pm 50$ K, being way above the surface temperature of $T_s = 90$ K. From Boltzmann plots we deduce rotational temperatures of $T_R = 260$ and 470 K for the fast channel and $T_R = 410$ K for the slow channel, independent of the vibrational state. This is documented in the examples shown in Fig. 4, where we present Boltzmann plots of the fast and the slow channel for two vibrational states. Earlier we had assumed that the "fast" channel is due to nonthermal, and the "slow" channel due to thermally equilibrated, desorption processes. How-

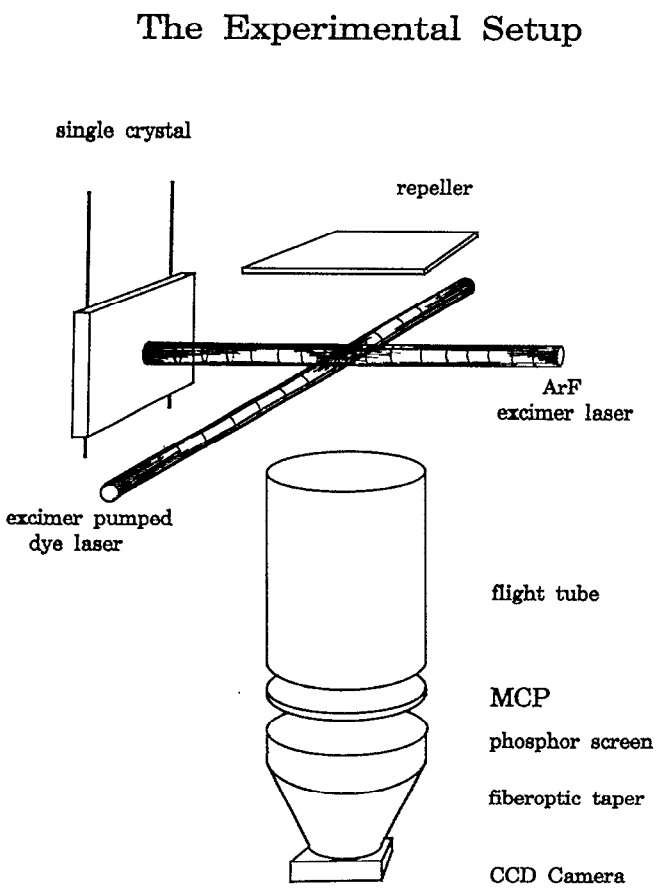

FIG. 2. Schematic representation of the experimental setup.

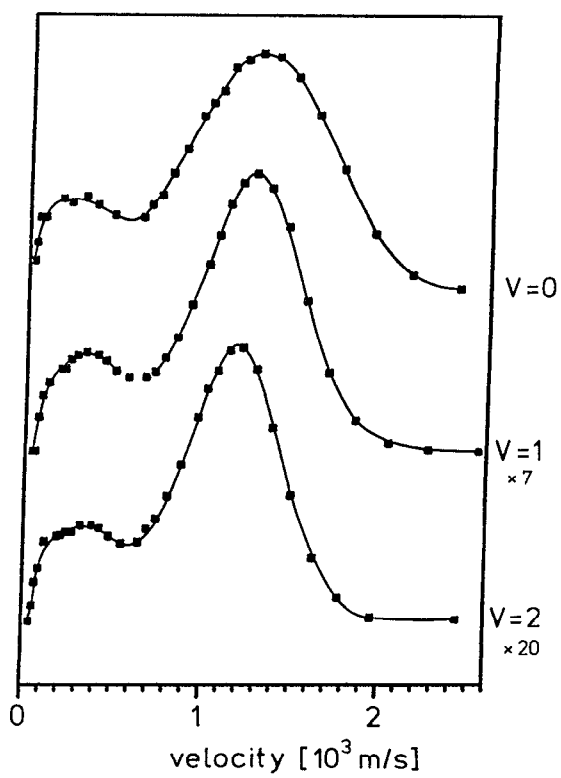

FIG. 3. Velocity flux distributions of a particular rotational state ($N = 10$) for three vibrational states.

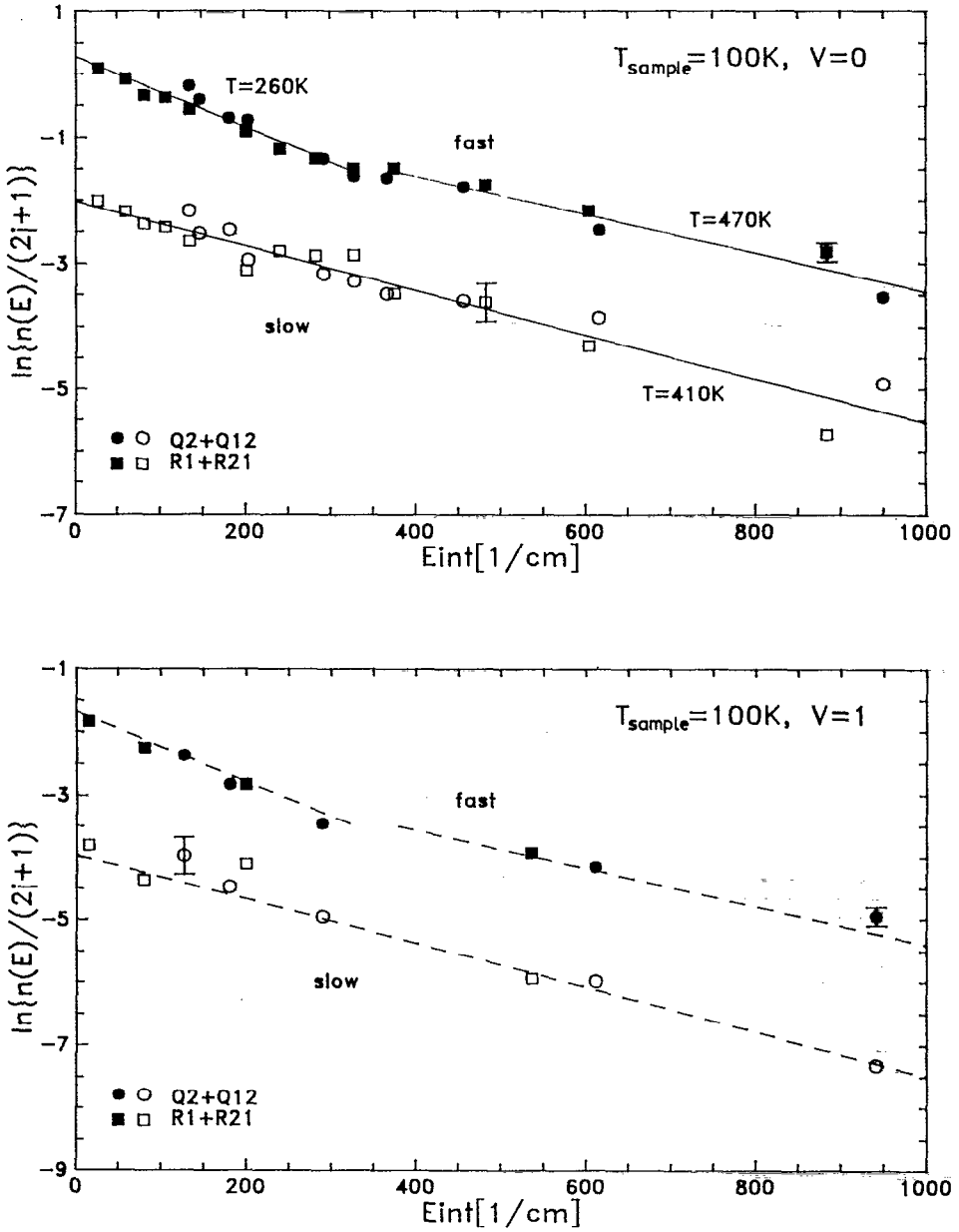

FIG. 4. Boltzmann plots for the rotational states of the fast and slow channels in $v=0$ and $v=1$.

ever, our present results indicate that both channels represent nonthermal processes.

Clearly, from our previous studies, especially the thermal desorption spectroscopy, high-resolution electron-energy-loss spectroscopy, and NEXAFS results, we know that there is a single terminally bound NO species present on the surface, whose molecular axis is inclined by about 40°–50° with respect to the NiO(100) surface normal. It must therefore be concluded that the bimodal distribution mirror images two different desorption channels of the same species.

III. THE DESORPTION MODELS

A framework to discuss DIET (desorption induced by electronic transitions) processes is the well-known MGR (Menzel–Gomer–Redhead) model.[19,20] Briefly, as indicated in Fig. 5, desorption is triggered by an electronic transition of the bound adsorbate–substrate complex. After the change of the potential-energy curve has occurred the molecule propagates under the influence of the new potential for a time τ and may accumulate kinetic energy. After the time τ has elapsed the system relaxes into the ground state and transfers potential energy to the solid substrate via electron-hole-pair creation and/or phonon coupling. If the Franck–Condon concept is applied the molecule keeps its kinetic energy, and if the accumulated kinetic energy is larger than the depth of the ground state well at the relaxation distance (Fig. 5) the molecule may escape the ground-state well and desorption occurs.

To consider the dynamics of the molecule in the adsorbed state we use the model of the rigid rotor, which appears to be justified as judged by the experimentally observed

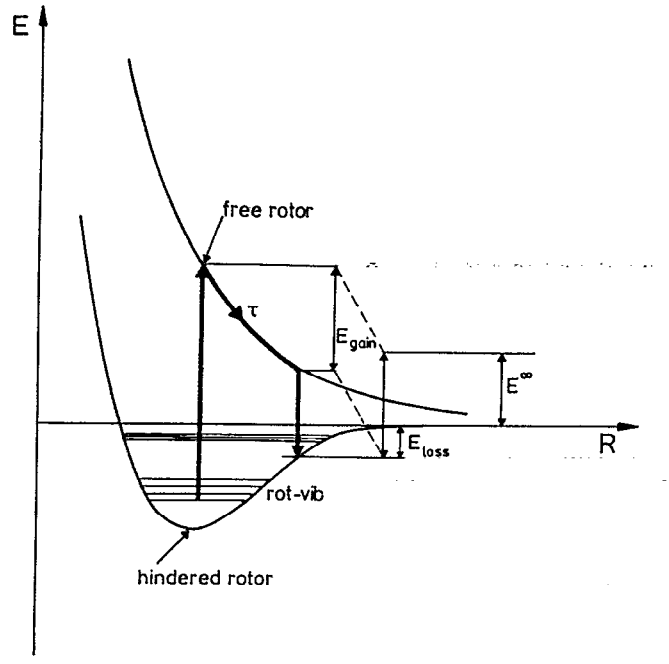

FIG. 5. Schematic representation of the MGR model for desorption. The thick arrows indicate the propagation of the molecule from the moment of excitation to the instant of relaxation. The energy values indicate the kinetic energy gained in the excited state (E_{gain}), the energy that needs to be overcome after relaxation has occurred (E_{loss}), and the kinetic energy of the desorbing particle (E_{∞}). R denotes the coordinate associated with the rupture of the surface molecule bond.

decoupling of the vibration and translation (see above). Figure 6(a) illustrates typical motions of a molecule bound to the NiO(100) surface: In addition to the molecule–surface vibration a bending vibration of the molecule with respect to the surface may be excited which is fixed in amplitude to a region of solid angles by the angular dependence of the ground-state potential [Fig. 6(a)]. Due to these and possibly other motions a momentum **k** may be associated with the

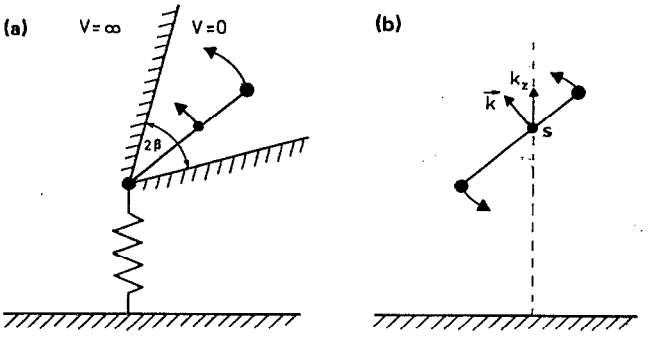

FIG. 6. Schematic representation of a diatomic molecule bound with bent geometry to a substrate surface. (a) The molecule is allowed to vibrate with respect to the surface indicated by a spring. In addition, the molecule performs a bending mode within a cone bordered by an infinitely high potential-energy wall. (b) The motion of the nonbonded molecule may be described by the rotation about the center of mass (S) and by the translation of the center of mass indicated by the vector **k**.

center-of-mass motion of the molecule in the ground state which is conserved during the electronic excitation of the molecule–surface complex. With the assumption of an isotropic excited-state potential, the electronic excitation leads to a rupture of the molecule–surface bond, i.e., the hindered rigid rotor in the adsorbed state becomes a free rigid rotor in the excited state. The translational motion of the center of mass of the molecule may be characterized by the vector **k** [Fig. 6(b)]. In case the electronic excitation occurs during the motion of the molecule away from the surface, **k** has a component pointing along the positive direction of the surface normal (k_z); in case it occurs while moving toward the surface, **k** has a component pointing along the negative direction of the surface normal. The different signs of the k_z components have consequences for the desorption dynamics: For a repulsive excited potential molecules with positive k_z components are readily moving away from the surface, while molecules with negative k_z are primarily moving toward the surface. After the initial momentum has been converted to potential energy, the molecules turn around and move outward. Therefore, if the same lifetime in the excited state is chosen for all desorbing molecules, a molecule with an initially negative k_z component cannot acquire as much kinetic energy as a molecule with positive k_z. Consequently, relaxation to the ground state occurs at different positions on the potential-energy surface, and thus the desorption dynamics will be different, which can lead, for example, to bimodal velocity (momentum) distributions (as is shown in Appendix C for a special case). In other words, for a short lifetime of the excited state the relaxation occurs for both distributions at nearly the same position of the potentials and with nearly the same absolute values for k_z, resulting in one peak of the momentum distribution after desorption. For longer lifetimes the relaxation of the two distributions occurs at different positions and with different absolute values of k_z, resulting in bimodal momentum distributions.

Analogous considerations for a purely attractive excited potential may not or may also lead to bimodal velocity distributions. Generally, however, the observed behavior strongly depends on the details (e.g., slope, existing minima, etc.) of the chosen excited-state potential (see below).

What is the nature of the repulsive potential-energy curve? This is a difficult problem but one might try to tackle it by asking a slightly modified question: Can we think of a potential-energy surface created by considering reasonable, physical elementary steps? Let us assume as the first elementary step the creation of an electron-hole pair which initiates the electron to be charge transferred from the substrate to the molecule. In the literature there are some experimental indications that this is the situation encountered at the surface.[14] The excited-state wave function of the adsorbed molecule would then look like a state of the NO anion. The remaining positive hole on the substrate, possibly on the Ni initially, is screened on the oxide surface via the mobile electrons of the oxygen sublattice. In other words, the molecular ion may feel an image charge which may lead to an excited-state potential with a minimum, the position of which depends on the details of the electronic interaction. However, upon excitation we assume that the molecules only probe the

repulsive part of the excited-state potential because of the short lifetime on the potential-energy curve. Therefore, we simulate this part of the potential curve by a repulsive $1/r$ potential. We describe the rotational motion of the molecules on the excited-state potential as a free rotor: If the interaction is basically electrostatic in nature it is reasonable to assume it to be isotropic. Therefore, in general, the motion is thought to be more similar to a free than to a hindered rotor. Note, however, that the angular space probed by the molecule is small ($\Delta\theta \leqslant 30°$) because the molecule has no time to fully rotate in the excited state.

So far we have neglected the vibrations of the NO molecule in the adsorbate as well as in the desorbing particles. Our experimental results indicate that we can assume complete decoupling of rotation and translation from vibration. If we furthermore assume that the NO stretching vibration is decoupled from the NO–metal vibration we may find simple qualitative arguments to explain the observed vibrational excitations of the desorbing molecules (see Sec. II). The situation is depicted in Fig. 7 where two potential-energy surfaces (ground and excited states) are plotted as a function of the two independent degrees of freedom, namely the motion of the molecule away from the surface (R) and the NO stretching motion (r). The excitation process may be described as follows: Before excitation the molecule is located in the global minimum of the lower curve. The photon excites the system via a Frank–Condon–like transition into the upper surface where the system only exhibits a minimum with respect to the NO stretching motion (r) and no minimum with respect to R. However, the position of the minimum as well as its shape differs from the situation in the r direction on the ground-state potential-energy surface. If we choose the potential-well minimum to be located at larger distance, as would be the case if the nature of the excited state is NO^- like, the excitation leads to a noneigenstate of the excited system in general. The propagation of this noneigenstate may be described by solving the time-dependent Schrödinger equation. It is our problem to find the probability that after a time τ, when relaxation occurs to the ground state, the system is in the nth vibrational state on the ground potential-energy surface. Under the assumption that the vibrations are described by harmonic oscillators, these probabilities are given by[18]

$$|\langle n_1|\psi_2(\tau)\rangle|^2 = \left|\sum_{n_2} \exp[-i(n_2 + \tfrac{1}{2})\omega\tau]\langle n_1|n_2\rangle\langle n_2|0_1\rangle\right|^2, \quad (1)$$

where the indices 1 and 2 characterize the ground- and excited-state harmonic oscillators, $\psi_2(\tau)$ the noneigenstate after excitation, n_1 and n_2 the quantum numbers of the two involved harmonic oscillators, ω the quantum energy in state 2, and 0_1 characterizes the ground-state zero-point harmonic oscillator. We assume to have significant quantum-state populations at the surface just for $v = 0$. Choosing ω from experimental data of various excited NO, or NO^+ and NO^- ground states, we may determine a relaxation time τ after which, for example, the experimentally determined vibrational populations of the desorbing molecules are reproduced.

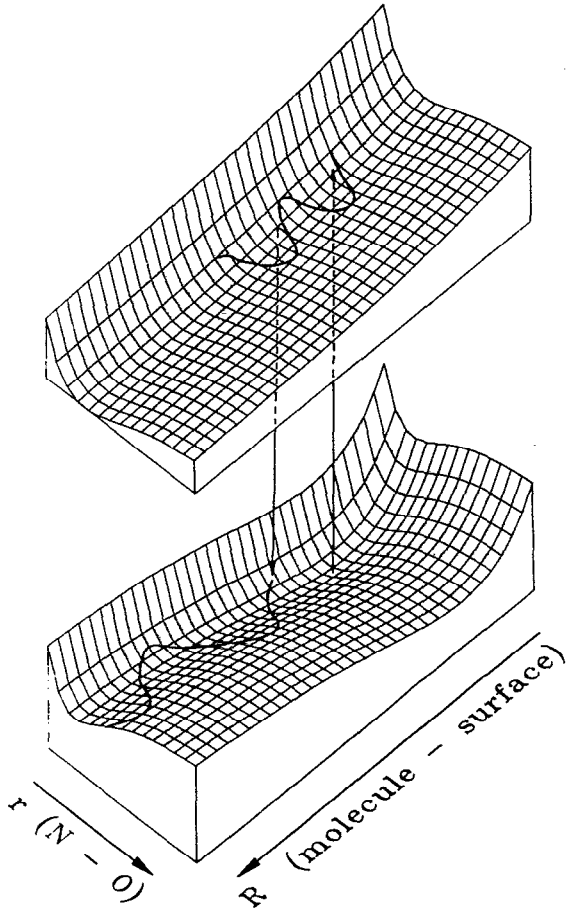

FIG. 7. Schematic representation of the potential-energy surfaces involved in the vibrational excitation process.

IV. COMPUTER SIMULATIONS FOR THE SIMPLEST CASES AND DISCUSSION

To test the model considerations presented at the beginning of the last paragraph we have carried out trajectory calculations. Within the framework of the MGR model two potential-energy surfaces are needed which model the adsorbate–substrate interactions. Furthermore, we have to determine probabilities for the transitions between the potential-energy surfaces. The potential-energy surface for the electronic ground state is modeled with a potential proposed in the literature.[21] We have incorporated in the potential the tilting of the NO molecules and the adsorption energy, i.e., the depth of the potential well as estimated from TPD data.[17]

To keep our approach as simple as possible we have chosen a $1/r$ potential for the excited state and not incorporated an angle dependency, though Hasselbrink[13] has mentioned that the coupling between linear and angular momentum in the fast desorption channel (Fig. 1) might be explained by this potential feature.

The transition probabilities between the potential-ener-

gy surfaces may then be written in a closed form (see Appendix B for details), if we describe the hindered rotation in the ground state by the above model [Fig. 6(a)], where the molecule may rotate freely within a given solid angle which is bordered by an infinitely high potential wall.[22] The solid angle may be chosen as a parameter of the calculation and has been set to 60° for the numerical results presented here. We have used 20 000–40 000 trajectories to calculate the momentum distribution for one lifetime of the excited state. (The scattering will be reduced if the number of calculated trajectories will be increased.)

In Fig. 8(a) a calculated momentum distribution assuming a lifetime τ in the excited state of about 4×10^{-14} s is plotted. As a result a bimodal velocity distribution is found. For an analysis of the nature of the bimodality we have restricted the calculation to only consider trajectories with $k_z>0$ or $k_z<0$ immediately after the excitation. In this case, the calculated distribution only contains the corresponding single maximum at higher or lower velocities, respectively. Figure 8(b) shows the dependence of the position of the maxima as a function of the lifetime τ of the molecule in the excited state.

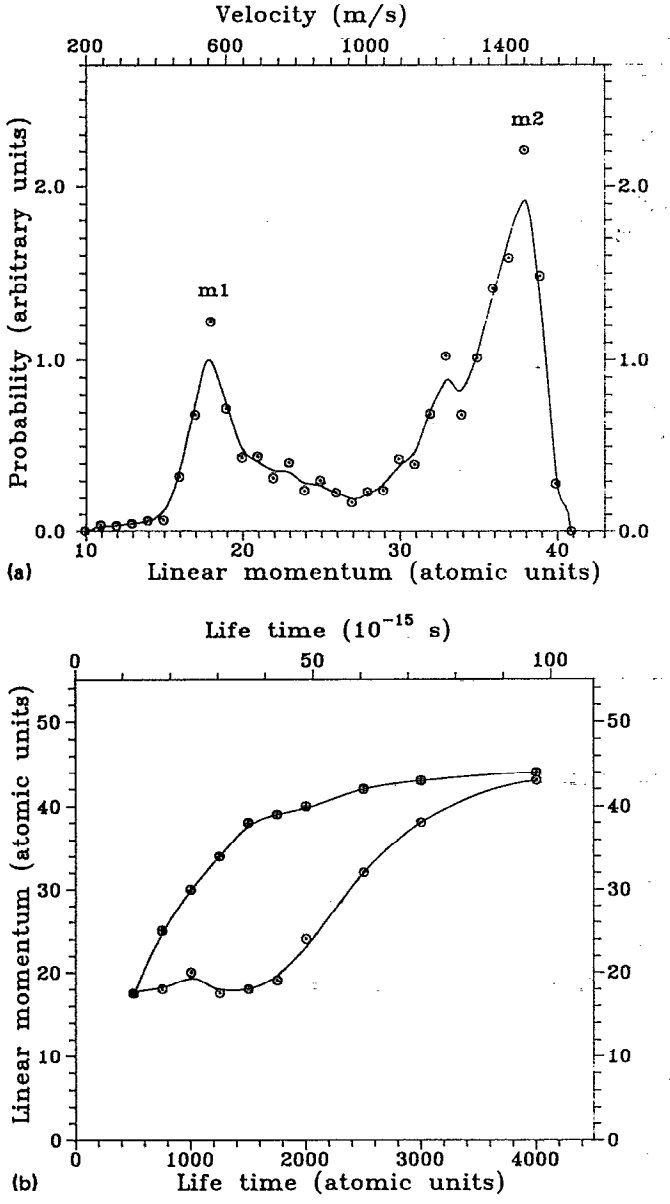

FIG. 8. Results of the model calculations. (a) Distribution of linear momenta calculated with a lifetime τ of 1500 a.u. (equal to 4×10^{-14} s). (b) Position of the maxima ($m1$, $m2$) in (a) as a function of the lifetime in the excited state. Through the data points we have drawn smoothed solid lines to guide the eye.

The calculated and measured velocity distributions both show bimodal velocity distributions in agreement with expectations based on the above desorption model. Note that in order to be able to observe bimodal distributions (i.e., the maxima are well separated) the model asks for a certain lifetime in the excited state. For metal surfaces, for example, relatively short lifetimes of $\tau\approx10^{-15}$ s have been deduced.[13,14] If we introduce such values into our model we find only one maximum in the calculated velocity distribution. This is in agreement with observations on metal surfaces and also with model simulation.

The behavior of the upper curve in Fig. 8(b) ("fast" maximum) directly follows from what has been said about the desorption model: A longer lifetime of the excited state is correlated with more kinetic energy in the desorbing molecule. It is not so easy to correctly predict the detailed behavior of the lower curve (i.e., the maximum at lower velocities). However, it is obvious that the structure in the curve depends on the details of the ratio of the slopes of the two potentials involved in the desorption process.

The simulation for the measured vibrational excitations is based on the model assumptions discussed in Sec. III. Appendix D contains the details of the calculations. Choosing the frequency of NO^- either for a very short time (i.e., 2×10^{-15} s) or after the molecule has undergone one or n numbers of vibrational cycles (i.e., 3×10^{-14} s, 6×10^{-14} s, etc.), the measured numbers are reproduced. A classical trajectory in the excited potential-energy curve is schematically indicated in Fig. 7. In this case the deexcitation is arbitrarily chosen to occur near completion of the first vibrational cycle. The relaxation time τ for the vibrational mode is under these conditions comparable with the one determined via analysis of the rotational and translational motions. The vibrational excitation in the ground state is schematically drawn as a wiggly line. One question to ask here is, why should the relaxation times of the vibrational motion and the translational–rotational motion be similar? If the excited state of the system involves a NO^- species then the electron has to be transferred back into the substrate before the molecule leaves the surface in the neutral ground state. This is triggered by the motion of the molecule away from the surface, because there has to be some overlap for the electron to be transferred back. The latest time is of the order of several 10^{-14} s.

V. SYNOPSIS

Fully state-resolved detection of UV-laser-induced desorption of NO from NiO(100) at $T=90$ K indicates the presence of bimodal velocity distributions. The measure-

ments reveal that both channels are caused by nonthermal processes and that the internal degrees of freedom, i.e., rotation, vibration, and translation are widely decoupled. The desorbing molecules are highly vibrationally excited corresponding to a temperature close to 2000 K.

We have carried out trajectory calculations to simulate the desorption processes, and these calculations allow us to suggest an explanation for the existence of bimodal velocity distributions: In a classical picture the two maxima are connected with the instant at which the molecule surface bond of the system vibrating with respect to the surface is ruptured. The maximum at high velocities is assigned to molecules moving away from the surface when the electronic excitation occurs; the maximum at low velocities is due to molecules excited on the way toward the surface. The velocity difference between the two maxima depends on the lifetime of the molecule in the excited state.

The observed vibrational populations of the desorbing molecules are described by model calculations assuming the intermediate formation of a negative NO ion. The longer N–O equilibrium bond length in NO^- as compared to neutral NO in the ground state is responsible for the vibrational excitation in our model. We estimate a relaxation time for the vibrational processes which is compatible with the rotational–translational relaxation time of 4×10^{-14} s.

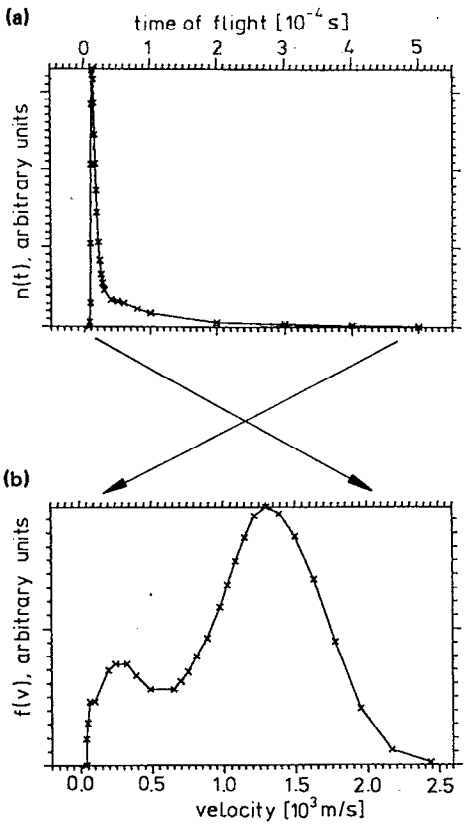

FIG. 9. (a) TOF distribution. (b) Velocity distribution.

ACKNOWLEDGMENTS

We thank the Deutsche Forschungsgemeinschaft, the Ministerium für Wissenschaft und Forschung des Landes Nordrhein-Westfalen, and the Fonds der chemischen Industrie (H.J.F.) for financial support. The Höchstleistungsrechenzentrum der KFA Jülich is gratefully acknowledged for providing the necessary computer time on a Cray Y-MP computer. We thank R. Schinke and K. Weide for the original version of the computer program solving the classical equation of motion problem. The discussions with V. Staemmler were helpful in understanding the origin of the bimodal distributions.

APPENDIX A

We measure in our experiments time-of-flight distributions. One example is shown in Fig. 9(a). $n(t)$ is the REMPI signal intensity of all the ions produced in a distance ranging from 15 to 18 mm normal to the surface. The long decay of the signal indicates the existence of more than one desorption channel. This fact becomes evident if we regard the corresponding velocity distribution presented in Fig. 9(b). The transformation is given by

$$f(v) = n(t)\times t. \tag{A1}$$

Now we clearly distinguish two maxima. For discussion we use velocity distributions instead of time-of-flight distributions throughout this paper.

The greatest error in the determination of the velocity is the uncertainity ($\pm$ 0.5 mm) in the distance of the center of the exciting laser beam from the surface. Therefore the error of the velocity is about 3%. The intensity of the REMPI signal is averaged over 10 laser pulses. With an error of 10% for a single pulse we estimate an error of 3% in the averaged REMPI intensity. Consequently, we have not drawn error bars in Figs. 1 and 9.

APPENDIX B

According to Landman,[22] the transition probability between given states of the hindered and a free rigid rotor may be written as

$$W(l,m_l,\mathbf{k},\nu,m_\nu,\beta) = N\frac{1}{Z_{\text{hin}}}\exp\left[\frac{-B_{\text{hin}}\times\nu\times(\nu+1)}{k_b\times T}\right] \times|\langle l,m_l,\mathbf{k}|\nu,m_\nu,\beta\rangle|^2\delta_{\text{energy}}, \tag{B1}$$

where l and m_l are the quantum numbers of the free rotor, and k characterizes the center-of-mass motion of the desorbing particle. Here, ν and m_ν are the corresponding quantum numbers of the hindered rigid rotor and β is half the solid angle for the hindered motion [see Fig. 6(a)]. N is a normalization factor, Z_{hin} is the partition function of the hindered rotor with a rotational constant B_{hin}. k_B is the Boltzmann factor and T the temperature. δ_{energy} is introduced to guarantee energy conservation. It includes the potential, translational, and rotational energies of both states which are involved in the transition.

The matrix elements are integrals of the initial (hindered rotor) and final state (free rotor) wave functions,

$$\psi_i = N_i \sum_{l=|m_l|}^{\infty} \langle l,m_l|v,m_v,\beta\rangle Y_{l,m_l}(\theta,\phi) \times\delta(R-d)\delta(\hat{R}-\hat{r})\delta(r-a) \quad \text{(B2)}$$

and

$$\psi_f = N_f \exp(i\,\mathbf{k}\cdot\mathbf{R}) \times Y_{l,m_l}(\theta,\phi), \quad \text{(B3)}$$

and may be represented as

$$\langle l,m_l,\mathbf{k}|v,m_v,\beta\rangle = N' \times\sqrt{2l+1}\times(-1)^{m_v} \sum_{l_1=0}^{\infty} (-i)^{l_1} \times Y_{l_1,m_v-m_l}(\theta_k,\phi_k)\times j_{l_1}(k\times d)\times(2l_1+1)^{1/2} \times \sum_{l_2=|m_v|}^{\infty} \langle l_2,m_v|v,m_v,\beta\rangle\times(2l_2+1)^{1/2} \times \begin{pmatrix} l & l_1 & l_2 \\ 0 & 0 & 0 \end{pmatrix} \times \begin{pmatrix} l & l_1 & l_2 \\ -m_l & m_l-m_v & m_v \end{pmatrix}. \quad \text{(B4)}$$

$Y_{l_1,m_v-m_l}(\theta_k,\phi_k)$ is a spherical harmonic which depends on two spherical coordinates of $\mathbf{k}$. $j_{l_1}(k\times d)$ is a spherical Bessel function depending on the length of $\mathbf{k}$ and a quantity d describing the distance between the center of mass and the apex of the cone [see Fig. 6(a)]. N' is a second normalization constant and the two brackets at the end represent Wigner $3j$ symbols.

APPENDIX C

In this appendix we show for a special case, i.e., the hindered rotor in half space ($\beta = 90°$, Fig. 10), that for excitation from the lowest rotational state of this rotor into the lowest state of the free rotor we have to expect a bimodal distribution of linear momenta immediately after the excitation.

The probability for excitation is governed by the expression (B4) in Appendix B. The quantum numbers for the lowest state of the free rotor are $l = m_l = 0$, while for the hindered rotor with $\beta = 90°$ it is $v = 1$, $m_v = 0$. $v = 1$ accounts for the boundary condition that the wave function with respect to the polar motion has to have a node at the plane of the potential step. For the product of the Wigner $3j$ symbols we end up with one term due to the conditions for l_1 and l_2:

$$\begin{pmatrix} 0 & l_1 & l_2 \\ 0 & 0 & 0 \end{pmatrix}^2 = \begin{cases} 0 & \text{if } l_1 \neq l_2, \\ 1/(2l_1+1) & \text{if } l_1 = l_2. \end{cases}$$

We find that

$$\langle l_2,m_v|v,m_v,\beta\rangle = \frac{1}{\sqrt{2}},$$

and the sum with index l_2 reduces to one term $l_1 = l_2 = v = 1$. With this Eq. (B4) reduces to

$$\langle l,m_l,\mathbf{k}|v,m_v,\beta\rangle = -iN_fN_i\sqrt{2\pi}d^2Y_{1,0}(\theta_k,\phi_k)j_1(k\times d).$$

Since

$$Y_{1,0}(\theta_k,\phi_k) = \sqrt{3/4\pi}\cos(\theta_k)$$

and

$$j_1(k\times d) = \frac{\sin(k\times d)}{(k\times d)^2} - \frac{\cos(k\times d)}{k\times d}$$

we find that $\langle l,m_l,\mathbf{k}|v,m_v,\beta\rangle \sim \cos(\theta_k)$. With $\cos(\theta_k) = k_z/k$, where k_z is the z component of the vector $\mathbf{k}$ with length k, we obtain

$$|\langle l,m_l,\mathbf{k}|v,m_v,\beta\rangle|^2 \sim k_z^2/k^2.$$

Since k is a constant given by energy conservation the probability is proportional to k_z^2; see Fig. 11.

This is a bimodal distribution of linear momenta for one particular rotational excitation. To calculate the full distribution many of such distributions, i.e., those which are populated according to the temperature and the resulting Boltzmann term, have to be averaged. Whether a bimodal or a monomodal velocity distribution is observed in the exit channel strongly depends on the number of transitions which have to be taken into account in the averaging process.

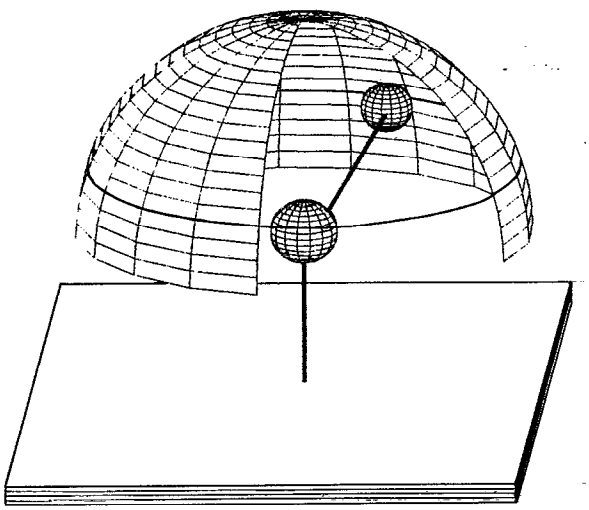

FIG. 10. Schematic representation of the hindered rotor with an opening angle of $\beta = 90°$.

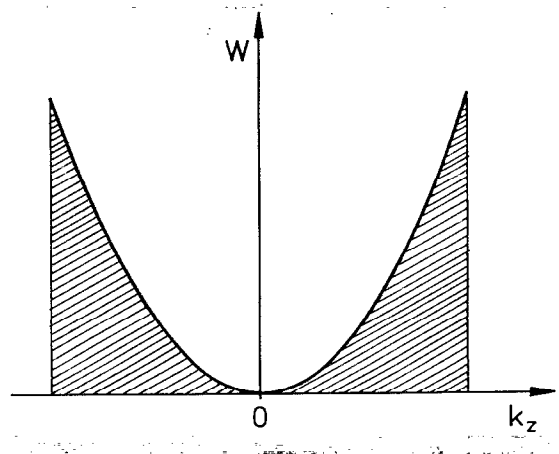

FIG. 11. The momentum distribution after the transition between the lowest rotational states is proportional to k_z^2. The range of possible values of k_z is restricted according to energy conservation.

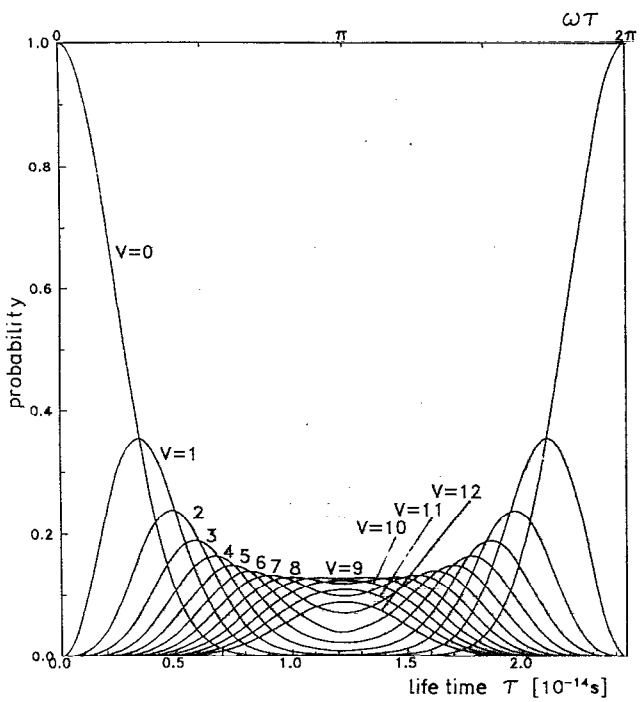

FIG. 12. Calculated relative populations of the vibrational states $v = 0$ to $v = 12$ of the desorbing molecules.

APPENDIX D

Equation (1) was solved by integrating products of harmonic-oscillator wave functions

$$\psi_v(x) \times \psi'_{v'}(x - \Delta a),$$

where $\Delta a = a_1 - a_2$ is the difference in equilibrium distances of the two harmonic oscillators (1, 2) and x is the vibrational coordinate. The individual harmonic-oscillator wave functions have the form

$$\psi_v(x) = \left(\frac{1}{2^v \times v! \times \sqrt{\pi}}\right)^{1/2} H_v(x) \left(\frac{\mu \times \omega}{\hbar}\right)^{1/4} \times \exp\left(\frac{-\mu \times \omega}{2\hbar} \times x^2\right),$$

where $H_v(x)$ are Hermite polynomials, μ the reduced mass, and ω the eigenfrequency. The integration was carried out numerically in the range $-0.3a_1 < x < 0.3a_1$ on a grid with separation $10^{-2}a_1$.

As a function of the relaxation time τ the probabilities for finding the system in $v = 0,\ldots,v = 12$ have been calculated and are plotted in Fig. 12. For the ground state an equilibrium distance of 1.150 77 Å and an eigenfrequency of 1904 cm^{-1} have been used. For the excited state the corresponding quantities were 1.258 Å and $\omega = 1363$ cm^{-1} as taken from Huber and Herzberg[23] for the ground state of NO^-.

[1] A. Mödl, H. Robota, J. Segner, W. Vielhaber, M. C. Lin, and G. Ertl, J. Chem. Phys. **83**, 4800 (1985).
[2] A. Mödl, T. Gritsch, F. Budde, T. J. Chuang, and G. Ertl, Phys. Rev. Lett. **57**, 384 (1986).
[3] D. Burgess, Jr., D. A. Mantell, R. R. Cavanagh, and D. S. King, J. Chem. Phys. **85**, 3123 (1986).
[4] A. R. Burns, E. B. Stechel, and E. R. Jennison, Phys. Rev. Lett. **58**, 250 (1987).
[5] D. Weide, P. Andresen, and H.-J. Freund, Chem. Phys. Lett. **136**, 106 (1987).
[6] F. Budde, A. V. Hamza, P. M. Ferm, G. Ertl, D. Weide, P. Andresen, and H.-J. Freund, Phys. Rev. Lett. **60**, 1518 (1988).
[7] W. C. Natzle, D. Padowitz, and S. J. Sibener, J. Chem. Phys. **88**, 7975 (1988).
[8] S. A. Buntin, L. J. Richter, D. S. King, and R. R. Cavanagh, J. Chem. Phys. **91**, 6429 (1989).
[9] E. Hasselbrink, S. Jakubith, S. Nettesheim, M. Wolf, A. Cassuto, and G. Ertl, J. Chem. Phys. **92**, 3154 (1990).
[10] M. Wolf, E. Hasselbrink, J. M. White, and G. Ertl, J. Chem. Phys. **93**, 5327 (1990).
[11] R. Schwarzwald, A. Mödl, and T. J. Chuang, Surf. Sci. **242**, 437 (1991).
[12] K. Mase, S. Mizuno, Y. Achiba, and Y. Murata, Surf. Sci. **242**, 444 (1991).
[13] E. Hasselbrink, Chem. Phys. Lett. **170**, 329 (1990).
[14] J. W. Gadzuk, L. J. Richter, S. A. Buntin, D. S. King, and R. R. Cavanagh, Surf. Sci. **235**, 317 (1990).
[15] Th. Mull, H. Kuhlenbeck, G. Odörfer, R. Jaeger, C. Xu, B. Baumeister, M. Menges, G. Illing, H.-J. Freund, D. Weide, and P. Andresen, *Desorption Induced by Electronic Transitions, DIET IV*, Vol. 19 in Springer Series in Surface Sciences (Springer-Verlag, Berlin, 1990), p. 169.
[16] B. Baumeister, M. Menges, T. Mull, H.-J. Freund, D. Weide, and P. Andresen, Proceedings of the Symposium on Surface Science, La Plagne, France, 1990 (unpublished), p. 147.
[17] H. Kuhlenbeck, G. Odörfer, R. Jaeger, G. Illing, M. Menges, Th. Mull, H.-J. Freund, M. Pöhlchen, V. Staemmler, S. Witzel, C. Scharfschwerdt, K. Wennemann, T. Liedtke, and M. Neumann, Phys. Rev. B **43**, 1969 (1991).
[18] Th. Mull, Ph. D. thesis (University of Bochum, 1991).
[19] D. Menzel and R. Gomer, J. Chem. Phys. **41**, 3311 (1964).
[20] P. A. Redhead, Can. J. Phys. **42**, 886 (1964).
[21] J. E. Smedley, G. C. Corey, and M. H. Alexander, J. Chem. Phys. **87**, 3218 (1987).
[22] U. Landman, Isr. J. Chem. **22**, 339 (1982).
[23] K. P. Huber and G. Herzberg, *Molecular Spectra and Molecular Structure. Vol. 4. Constants of Diatomic Molecules* (Van Nostrand Reinhold, New York, 1979).